Accepted for publication in ***Indoor Air*** (October 19, 2012)

On the suitability of steady RANS CFD for forced mixing ventilation at transitional slot Reynolds numbers

T. van Hooff [*] [a,b], B. Blocken [a], G.J.F. van Heijst [c]

[a] Building Physics and Services, Eindhoven University of Technology, P.O. Box 513, 5600 MB Eindhoven, The Netherlands.
[b] Building Physics Section, KU Leuven, Kasteelpark Arenberg 40, P.O. Box 2447, 3001 Leuven, Belgium.
[c] Fluid Dynamics Laboratory, Eindhoven University of Technology, P.O. Box 513, 5600 MB Eindhoven, The Netherlands.

Abstract

Accurate prediction of ventilation flow is of primary importance for designing a healthy, comfortable and energy-efficient indoor environment. Since the 1970s, the use of computational fluid dynamics (CFD) has increased tremendously and nowadays it is one of the primary methods to assess ventilation flow in buildings. The most commonly used numerical approach consists of solving the steady Reynolds-averaged Navier-Stokes (RANS) equations with a turbulence model to provide closure. This paper presents a detailed validation study of steady RANS for isothermal forced mixing ventilation of a cubical enclosure driven by a transitional wall jet. The validation is performed using particle image velocimetry (PIV) measurements for slot Reynolds numbers of 1,000 and 2,500. Results obtained with the renormalization group (RNG) k-ε model, a low-Reynolds k-ε model, the shear stress transport (SST) k-ω model and a Reynolds stress model (RSM) are compared with detailed experimental data. In general, the RNG k-ε model shows the weakest performance, whereas the low-Re k-ε model shows the best agreement with the measurements. In addition, the influence of the turbulence model on the predicted air exchange efficiency in the cubical enclosure is analyzed, indicating differences up to 44% for this particular case.

Keywords: forced mixing ventilation; computational fluid dynamics (CFD); transitional flow; particle image velocimetry (PIV); model validation; steady Reynolds-averaged Navier-Stokes (RANS)

Practical implications

This paper presents a detailed numerical study of isothermal forced mixing ventilation driven by a low-velocity (transitional) wall jet using steady computational fluid dynamics (CFD) simulations. It is shown that the numerically obtained room airflow patterns are highly dependent on the chosen turbulence model and large differences with experimentally obtained velocity fields can be present. The renormalization group (RNG) k-ε model, which is commonly used for room airflow modeling, shows the largest deviations from the measured velocities, indicating the care that must be taken when selecting a turbulence model for room airflow prediction. As a result of the different predictions of the flow pattern in the room, large differences are present between the predicted air exchange efficiency obtained with the four tested turbulence models, which can be as high as 44%.

1. Introduction

Ventilation is used to provide a healthy, comfortable, sustainable and energy efficient indoor environment in buildings, airplanes, cars, etc., by removing pollutants, excess heat and moisture, etc. The accurate prediction of ventilation flow is therefore of primary importance. The ventilation flow in an enclosure can be assessed by analytical and/or semi-empirical formulae, by full-scale or reduced-scale experiments or by numerical simulation using computational fluid dynamics (CFD). An overview of ventilation assessment methods is provided by Chen (2009). All methods should be conducted with the utmost care; an incorrect prediction of the ventilation flow in an enclosure will lead to incorrect predictions of the actual ventilation performance, e.g. the air exchange efficiency.

[*] **Corresponding author:** Twan van Hooff, Building Physics and Services, Eindhoven University of Technology P.O.Box 513, 5600 MB Eindhoven, the Netherlands. Tel.: +31 (0)40 247 5877, Fax +31 (0)40 243 8595.
E-mail address: t.a.j.v.hooff@tue.nl

Since the early work of Nielsen (1973) in the nineteen-seventies, a lot of work has been published on the numerical prediction of room airflow, which is governed by recirculation cells, flow separation and flow attachment (e.g. Awbi 1989, Jones and Whittle 1992, Kato et al. 1992, Gan and Awbi 1994, Nielsen 1998, van Hooff and Blocken 2010, Ramponi and Blocken 2012, Cao and Meyers 2012). The majority of these studies consisted of CFD simulations of mixing or displacement ventilation, either with or without buoyancy effects. Although it is widely recognized that large eddy simulation (LES) is inherently more accurate for ventilation flow modeling, its high computational cost is the main reason why the majority of ventilation studies is still performed using steady Reynolds-averaged Navier-Stokes (RANS) simulations. However, the use of steady RANS for room airflow modeling is challenging because of three distinct features of indoor airflow: (1) transitional flow; (2) turbulence anisotropy and; (3) adverse pressure gradients.

The first challenge is the modeling of transitional room airflow. Although the vast majority of the ventilation studies have been conducted for fully turbulent flow, transitional flow can be present in different types of room airflow, either in the supply jet region or in other regions of low velocities (e.g. corners of the room, vicinity of buoyant plumes) (e.g. Chen and Jiang 1992, Murakami et al. 1994, Li and Nielsen 2011). However, to the knowledge of the authors, only a limited number of ventilation studies have dealt with room airflow at transitional slot Reynolds numbers. Nielsen et al. (2000), Davidson et al. (2000) and Wang and Chen (2009, 2010) studied transitional room air flow experimentally and numerically. Davidson et al. (2000) concluded that only LES was capable of reproducing this type of room airflow based on the experiments by Nielsen et al. (2000). However, Wang and Chen (2009, 2010) concluded that steady RANS in combination with the renormalization group (RNG) k-ε turbulence model provided accurate results, which indicates the lack of consensus on the ability of steady RANS to model transitional room airflow. An overview of studies on transitional jets in other research areas is provided by van Hooff et al. (2012a).

The second challenge is the presence of turbulence anisotropy. In the RANS approach, the Reynolds decomposition leads to six additional terms in the RANS equations; the Reynolds stresses. These Reynolds stresses need to be modeled, which can be done by the Boussinesq hypothesis or by solving transport equations for each of the Reynolds stresses (i.e. second-order closure models, e.g. Reynolds stress models (RSM)). The most commonly used turbulence models based on the Boussinesq hypothesis are the linear two-equation eddy-viscosity models such as the k-ε and k-ω models. The Boussinesq hypothesis relates the Reynolds stresses to the mean velocity gradients by using an eddy (or turbulent) viscosity μ_t. An important approximation of the Boussinesq hypothesis is that it assumes the anisotropic part of the Reynolds stress tensor to be aligned with the shear stress tensor, presuming that a spatially dependant proportionality factor (i.e. the eddy viscosity) exists. This is mainly problematic in regions of high shear, where turbulence tends to be strongly anisotropic. It should be noted that in several publications it has been erroneously reported that the normal Reynolds stresses predicted by eddy-viscosity models are equal (= isotropic). The normal Reynolds stresses consist of an isotropic part (= 2/3k) to ensure that the sum of the normal Reynolds stresses always has the correct physical value, and an anisotropic part, which is only zero in case there is no shear in the flow. If shear is present the normal stresses are not equal due to unequal values of $\partial u/\partial x$, $\partial v/\partial y$ and $\partial w/\partial z$. Using a second-order closure model, e.g. RSM, one can more accurately take into account the effect of the Reynolds stresses on the flow field, which should provide superior results for these flows (e.g. Hanjalić 1994, Murakami et al. 1994, Schälin and Nielsen 2004). However, using RSM entails several disadvantages: increased computational demand and less straightforward convergence.

Finally, the third challenge for room airflow modeling using steady RANS is the presence of an adverse pressure gradient. In mixing ventilation flows a high-momentum jet is used to drive a recirculation region in the enclosure (e.g. Awbi 2007). The wall opposite to the ventilation opening from which the air jet is released into the enclosure, invokes an adverse pressure gradient. The higher pressure in the downstream top-corner of a room can induce the separation of the boundary layer (attached wall jet). The correct modeling of boundary layer separation (jet detachment) due to an adverse pressure gradient is not straightforward for some of the steady RANS models, i.e. high-Reynolds k-ε models (e.g. Patel et al. 1985, Rodi and Scheuerer 1986, Wilcox 1993, Casey and Wintergerste 2000, Chen and Srebric 2002). This inability is due to the fact that the HR k-ε models underpredict the turbulence dissipation rate ε, which is too small relative to the production rate of k. This leads to an incorrect eddy viscosity and an increased shear stress level near the wall, which leads to an unrealistic delay, or even prevention, of boundary layer separation. The k-ω models in general (e.g. Casey and Wintergerste 2000), and the shear stress transport (SST) k-ω model in particular (Menter 1993, Wilcox 1993, Menter 1996) are known to provide more accurate results in separating flows. Finally, second-order closure models, e.g. RSM, are said to provide superior predictions for flows in confined rooms with an adverse pressure gradient (Moureh and Flick 2003, 2005, Norton et al. 2007).

Although a lot of guidelines have been published on room airflow modeling (e.g. Nielsen 1990, 1998, 2004, Baker et al. 1994, Chen 1995, 1996, Chen and Srebric 2002, Sørensen and Nielsen 2003, Zhai et al. 2007, Zhang et al. 2007), no clear consensus could be found in literature on which turbulence models should be used for room airflow modeling in general, and for transitional room airflow in particular. This is at least partly attributed

to the large variety in indoor geometry and physical conditions in previous studies and to the large number of parameters influencing the airflow patterns.

The objective of this study is to assess the accuracy of steady RANS CFD simulations in combination with four frequently used turbulence models for forced mixing ventilation at transitional slot Reynolds numbers (i.e. $Re \approx 1{,}000$ and $Re \approx 2{,}500$) in a cubical enclosure driven by a wall jet. The study in this paper focuses on the three challenges mentioned above: (1) transitional flow, (2) turbulence anisotropy and (3) adverse pressure gradients. In Section 2, the experimental setup for the particle image velocimetry (PIV) measurements that are used for CFD validation is described. The computational model is described in Section 3 and Section 4 presents the steady RANS simulations for two slot Reynolds numbers ($Re \approx 1{,}000$ and $Re \approx 2{,}500$) and their comparison with the PIV measurements. The influence of the turbulence models on the predicted ventilation efficiency is shown in Section 5. A discussion with an overview of future work (Section 6) and conclusions (Section 7) conclude the paper.

2. PIV measurements

2.1 Reduced-scale model

A reduced-scale and water-filled model (1:6.67) of a 2 x 2 x 2 m^3 air-filled enclosure has been built to perform flow visualizations and PIV measurements. The former were conducted to determine the slot Reynolds numbers for which the studied flow is transitional, while the latter were performed to analyze the flow behavior and to obtain a data set for the validation of CFD models (van Hooff et al. 2012a, 2012b). The reduced-scale experimental setup is filled with water and consists of (1) a water column to drive the flow; (2) a flow conditioning section; (3) a cubic test section with dimensions 0.3 x 0.3 x 0.3 m^3 (L^3); and (4) an overflow (Fig. 1). The conditioning section in front of the inlet consists of one honeycomb, three screens and a contraction to obtain a uniform water flow at the inlet and to minimize the turbulence level. The test section has edges of 0.3 m (L) and is constructed from glass plates with a thickness of 8 mm. The inlet width (w) is 0.3 m ($w/L = 1$) and the inlet height (h) can be varied up to 0.03 m ($0 < h/L \leq 0.1$); for this study h/L is fixed to 0.1. The height of the outlet is fixed at $h_{outlet}/L = 0.0167$. The slot Reynolds number is defined based on the inlet height as $Re = U_0 h/\nu$, with U_0 the area-averaged inlet velocity based on the volume flow rate through the inlet and ν the kinematic viscosity at room temperature (≈ 20°C). The maximum local velocity U_M is used to make the velocities non-dimensional (U/U_M) (Fig. 1b). Note that U_M is defined as the local maximum time-averaged x-velocity, and thus varies with both x/L and Re. More information on the experimental setup can be found in van Hooff et al. (2012b).

2.2 PIV measurement setup

The PIV measurements were conducted using a 2D PIV system consisting of a Nd:Yag (532 nm) double-cavity laser (2 x 200 mJ, repetition rate < 10 Hz) used to illuminate the field of view, and one CCD (Charge Coupled Device) camera (1376 x 1040 pixel resolution, 10 frames/s) for image acquisition. The laser was mounted on a translation stage and was positioned above the cubic test section to create a laser sheet in the vertical center plane of the cube; the camera was positioned perpendicular to the water cube. Seeding of the water was provided by hollow glass micro spheres (3M; type K1) with diameters in the range of 30 – 115 μm.

Two sets of PIV measurements were performed in the vertical center plane ($z/L = 0.5$) of the water cube. The first set of measurements consists of data in the entire cross-section of the cube, i.e. a region of interest (ROI) of 0.3 x 0.3 m^2 (= ROI1). The second set contains PIV measurements in a smaller area of 0.18 x 0.12 m^2 (W x H) in the proximity of the inlet, enabling a higher measurement resolution (= ROI2). The uncertainty of the measurement results is around 2-4% in the largest part of the test section and is slightly higher in the shear layer and boundary layer areas as a result of the locally higher turbulence levels. For this study, the time-averaged velocities were used. Note that the results for $y/L < 0.05$ are not used in the remainder of this paper. The results in this part of the cube are inaccurate due to reflections of the laser sheet on the glass bottom of the cube. Additional information and measurement results can be found in van Hooff et al. (2012a).

3. CFD simulations

3.1 Computational geometry and grid

The computational model is a replica of a part of the experimental setup as described in Section 2.1. The conditioning section is not included in the model, only the contraction upstream of the inlet of the test section

has been taken into account (Fig. 2a). The outlet is extended in the x-direction to enhance convergence of the simulations. The computational grid was created using the surface-grid extrusion technique presented in van Hooff and Blocken (2010). A grid-sensitivity analysis was conducted using three different fully structured grids, ranging from 1,254,400 cells to 10,022,400 cells, based on a grid refinement of $\sqrt{2}$ in each direction (Fig. 2b, Fig. 3). The grid-sensitivity analysis was only performed for $Re \approx 1{,}000$ and with the SST k-ω model by Menter (1994). The three different grids are depicted in Figure 3, clearly illustrating the higher grid resolution in the boundary layer and the shear layer, which are the regions with high velocity gradients. The number of cells over the inlet height is 40, 56 and 80 for the coarse, middle and fine grid, respectively. Over the outlet height 20, 28 and 40 cells are present for the three different grids. An overview of the grid size and the corresponding dimensionless wall distances y^* at the top surface ($y/L = 1$) in the center plane are shown in Table 1. The y^* values range from 0.045 to 0.45 for the coarsest grid to 0.007 to 0.28 for the finest grid. The low values for y^* enable the use of low-Reynolds number modeling (LRNM), which implies solving the flow all the way down to the viscous sublayer. The grid resolution for the application of LRNM should be very fine, preferably with y^*-values at the wall-adjacent cell equal to or lower than 1. Note that using wall functions would reduce the near-wall grid resolution, and thus the computational demand, to a great extent since the center point of the wall-adjacent cell should be located in the log-law region ($y^* \approx 30$-300). However, the numerical accuracy using LRNM is larger than when using wall functions, in which semi-empirical formulae are used to bridge the region from the wall to the center of the wall-adjacent cell. Accurately resolving the flow all the way down to the viscous sublayer is especially important in situations in which low-Reynolds-number flow, pressure gradients and boundary layer separation are present, as is the case in this study.

The results of the grid-sensitivity analysis are shown in Figure 4, which shows the profiles of the non-dimensional x-velocities (U/U_M) in the vertical center plane ($z/L = 0.5$) at $x/L = 0.5$ and $x/L = 0.8$. It can be concluded that the results obtained with the coarse grid show some significant differences from those obtained with the middle grid. The results obtained with the middle grid and the fine grid nearly overlap, although there are still some small differences between the middle and the fine grid. Note that these differences are mainly present in the shear layer and boundary layer regions. The simulations for the grid-sensitivity analysis showed oscillatory convergence, comparable to that reported by Ramponi and Blocken (2012) and van Hooff et al. (2012c). The oscillations resulted in small fluctuations of the velocity, mainly in the wall jet region, which were within 2% and 5% of the average velocity at a given point for the two-equation models and the RSM model, respectively. To obtain an "average" solution the results were averaged over a sufficiently large number of iterations. More information can be found in the next subsection. Based on Figure 4, and taking into account the oscillatory convergence that was present, the middle grid was considered to provide fairly grid-independent results and is therefore used in the remainder of this study.

3.2 Boundary conditions

The boundary conditions were chosen to replicate those of the experiments as closely as possible. The surfaces were modeled as smooth no-slip walls. A uniform velocity was imposed at the CFD inlet (see Fig. 2a), which was based on the Reynolds number at the actual ventilation inlet during the experiments and the ratio between the height of the CFD inlet ($h/L = 0.3$) and the actual ventilation inlet ($h/L = 0.1$); $U_{inlet;CFD} = 0.01$ m/s for $Re \approx 1{,}000$ and $U_{inlet;CFD} = 0.025$ m/s for $Re \approx 2{,}500$. As a result of the contraction between the CFD inlet and the actual ventilation inlet, the velocities at the actual ventilation inlet are approximately three times higher than those imposed at the CFD inlet. The turbulence parameters were specified based on the hydraulic diameter and the turbulence intensity. The hydraulic diameter D_h was calculated using $D_h = (4WH)/(2(W+H))$, with H the height and W the width of the CFD inlet. The turbulence intensity (u_{RMS}/U_M) in the wall jet region at $x/L = 0.2$ was around 3-4% for each value of Re (van Hooff et al. 2012a). A constant turbulence intensity of 6% was imposed at the CFD inlet for $Re \approx 1{,}000$ and 18% for $Re \approx 2{,}500$. Due to the contraction the resulting turbulence intensity at the entrance of the cubic test section corresponded with the measured values (see Section 5.3). Zero static pressure was imposed at the outlet. Note that the boundary conditions were identical for all tested turbulence models to enable a fair comparison of their performance.

3.3 Solver settings

The 3D steady RANS simulations were conducted using Fluent 6.3.26 (Fluent 2006). Four different turbulence models were used to provide closure to the governing equations; three linear two-equation eddy-viscosity models (RNG k-ε, low-Reynolds k-ε, SST k-ω) and one second-order closure model (low-Re stress-omega Reynolds Stress Model). The standard k-ε model by Launder and Spalding (1974) has been used for engineering applications for several decades, however, it has several well-documented disadvantages (e.g. Casey and Wintergerste 2000) and was therefore not tested in this study. The RNG k-ε model by Yakhot et al. (1992) is an improved version of the standard k-ε model and has been extensively used in room air flow

modeling. In addition to the RNG k-ε model, the low-Reynolds number k-ε (LR k-ε) by Chang et al. (1995) was tested. This low-Re number turbulence model was designed for flow in a sudden expansion. Low-Re number models use damping functions to improve their accuracy in the near wall region and should show an improved performance for low-Re number flows as studied in this paper. The third turbulence model that was used is the SST k-ω model by Menter (1994). The eddy-viscosity function of the standard k-ω model has been adjusted for the SST model by Menter (1994), in order to account for the transport of the principal turbulent shear stress in adverse pressure gradient boundary layers. Finally, the low-Re stress-omega Reynolds Stress Model (RSM) by Wilcox (1998) was used. The RSM model is the only turbulence model tested in this study that solves transport equations for the individual Reynolds stresses and should show a better performance for the wall jet, since turbulence in a wall jet is anisotropic due to the damping effects of the wall. For all turbulence models studied in this paper the default model constants are used, which are not mentioned here for the sake of brevity. Note that most RANS turbulence models were developed for fully developed turbulent flow, which is not the case in this study. Flow visualizations indicated that transitional flow is present and that the measured turbulence intensities are very low (van Hooff et al. 2012a).

Pressure-velocity coupling is solved by the SIMPLEC algorithm, pressure interpolation is second order and second-order upwind discretization schemes are used for both the convection terms and the viscous terms of the governing equations. Convergence has been monitored carefully. For the majority of the simulations oscillatory convergence was present. As discussed in Ramponi and Blocken (2012) and van Hooff et al. (2012c), CFD simulations can exhibit oscillatory unsteadiness of the flow field, resulting in fluctuating values of the studied parameters as function of the number of iterations. Solely looking at the residuals is therefore not enough and might even be misleading. To obtain an "average" solution the results were averaged over a sufficiently large number of iterations. In this case, the averaging took place over an interval of 4,000 or an interval of 20,000 iterations, depending on the Re-value, grid size and the turbulence model.

4. Comparison of turbulence model performance

4.1 Velocities

The PIV measurements are compared with the numerical results obtained with steady RANS in combination with the four turbulence models described above. Figure 5 shows vertical profiles of U/U_M in the vertical center plane ($z/L = 0.5$) at $x/L = 0.2$, 0.5 and 0.8 (Fig. 5f) for $Re \approx 1{,}000$. Figures 5d,e show the results at $x/L = 0.2$ and $x/L = 0.5$ obtained from the PIV measurements in a smaller ROI (higher spatial resolution). At $x/L = 0.2$ the RNG k-ε model provides clearly erroneous predictions of U/U_M; the shape of the wall jet is not correct (not top-hat shaped) (Fig. 5d). Note that the experimentally obtained velocity profile in Figure 5a does not resemble a clear top-hat profile; this is due to the lower measurement resolution in ROI1 (van Hooff et al. 2012a). The other three turbulence models are able to predict the correct shape of the wall jet at this position. In Figure 5d it is shown that the LR k-ε model and the SST k-ω model also accurately predict the velocities below the wall jet ($0.7 < y/L < 0.9$), whereas the RSM model predicts too low x-velocities in this area. The results at $x/L = 0.5$ are depicted in Figures 5b and 5e. It can be seen that the RNG k-ε model provides the worst agreement with the measurement results. The wall jet is too thin and the location of maximum jet velocity is too close to the top surface. As seen in Figure 5a,d, the RSM model again predicts too small absolute x-velocities below the wall jet. Finally, Figure 5c shows the velocity profiles at $x/L = 0.8$. Although the LR k-ε model predicts too high negative x-velocities near the bottom of the cube, it shows the overall best agreement with the PIV measurements. The worst agreement is again obtained with the RNG k-ε model which underpredicts the jet detachment to a large extent. The SST k-ω and the RSM model on the other hand overpredict jet detachment compared to the measurements.

The profiles of U/U_M at $x/L = 0.2$, 0.5 and 0.8 for $Re \approx 2{,}500$ are depicted in Figure 6. The results at $x/L = 0.2$ for $Re \approx 2{,}500$ are quite similar to those for $Re \approx 1{,}000$. The shape of the wall jet is fairly accurate predicted by all models except by the RNG k-ε model, which again does not accurately predict the top-hat velocity profile at $x/L = 0.2$ (Fig. 6d). The RSM model again underpredicts the velocities below the wall jet ($0.7 < y/L < 0.9$) (Fig. 6a), whereas it predicts too large negative velocities between $y/L = 0.2$ and $y/L = 0.5$. Finally, the SST k-ω model predicts a positive velocity near the bottom surface, which is not in agreement with the measurements and is also not predicted by the other three models. From the measured profiles at $x/L = 0.5$ and $x/L = 0.8$ for $Re \approx 2{,}500$, it can be concluded that the jet separation from the top surface occurs further downstream in comparison with the results for $Re \approx 1{,}000$. This dependency on Re, as presented in van Hooff et al. (2012a), is not correctly reproduced by all turbulence models, which does not come as a surprise since most turbulence models are developed for fully developed turbulent flow (high Reynolds number). The velocity profiles obtained with the RNG k-ε model are almost the same as those for $Re \approx 1{,}000$ and again the wall jet detaches too far downstream. In contrast to the RNG k-ε model, the SST k-ω and the RSM model predict the jet detachment to

occur too far upstream resulting in deviations from measured profiles; the locations of maximum jet velocity are predicted to be too low at x/L = 0.5 and at x/L = 0.8 (Fig. 6b,c,e). The LR k-ε model in general provides the best agreement with the measurement results; the numerically obtained profiles closely resemble the measured velocity profiles, especially in the upper part of the cube. Near the bottom (y/L < 0.1), the LR k-ε model predicts too high negative values of U/U_M. In this area, the RSM model provides the best results. The fact that the results obtained with the RNG k-ε model for Re ≈ 2,500 show a better agreement with the measurement results than for Re ≈ 1,000, can be attributed to the higher measured turbulence level for Re ≈ 2,500, which delays the separation of the wall jet and which reduces the velocity gradient in the outer region of the wall jet (compare Fig. 5e and Fig. 6e). For even higher turbulence levels (higher values of Re), the performance of the RNG k-ε model will probably improve even further and probably will eventually show a good comparison with the measurements when the flow becomes fully turbulent.

4.2 Velocity vector fields

In addition to the detailed velocity profiles, also the velocity vector fields can be used to assess the performance of the turbulence models. Figure 7 shows the measured (Fig. 7a) and computed velocity vector fields in the vertical center plane (z/L = 0.5). The circular dot represents the measured center of the large recirculation zone, whereas the open circle represents the computed centers. It is again shown that the RNG k-ε model does not correctly predict the detachment of the wall jet due to the adverse pressure gradient. As a result, the smaller recirculation zone in the top-right corner is too small. Nevertheless, the computed center of the large recirculation zone does resemble the measured location quite well, but this is believed to be a coincidence since the other flow features do not correspond with the measurements. The location of the center of the recirculation zone is also fairly well predicted by the LR k-ε model (Fig. 7c) and the SST k-ω model (Fig. 7d). The former predicts the center to be slightly too far to the left, while the latter predicts a location that is slightly too high. These two turbulence models provide a more accurate prediction of jet detachment and of the resulting top corner recirculation zone. Finally, the RSM model shows quite a large deviation of the location of the center of the large recirculation zone; its shape clearly differs from the measured one. However, jet detachment is predicted quite accurately.

4.3 Turbulent kinetic energy

In addition to U/U_M, also the measured and predicted turbulent kinetic energy profiles can be compared, especially near the top surface. The turbulent kinetic energy is calculated using the measured root-mean-square (RMS) values in the longitudinal (u_{RMS}) and vertical direction (v_{RMS}), obtained with the PIV measurements in the reduced region of interest (ROI2), for improved spatial accuracy. Since the PIV measurements only provided the velocity components in the streamwise (U, u_{RMS}) and vertical direction (V, v_{RMS}), the RMS value in the lateral direction (w_{RMS}) is unknown. To be able to calculate the turbulent kinetic energy, the correlation between the normal stresses in a 2D wall jet, as described by Nielsen (1990), is used:

$$w_{RMS} \approx \sqrt{0.8}\, u_{RMS} \tag{1}$$

The turbulent kinetic energy can subsequently be calculated using

$$k = \frac{1}{2}\left({u_{RMS}}^2 + {v_{RMS}}^2 + {w_{RMS}}^2 \right) \tag{2}$$

Figure 8 shows the vertical profiles of k at x/L = 0.2 and at x/L = 0.5 for Re ≈ 1,000. The values of k predicted by the RNG k-ε model in the wall jet region are far too high in general, both at x/L = 0.2 ($k_{max} = 10^{-4}$ m^2/s^2) and x/L = 0.5 ($k_{max} = 7 \times 10^{-5}$ m^2/s^2). A closer look at Figure 8b shows that the RNG k-ε model strongly overpredicts the turbulent kinetic energy in the boundary layer at x/L = 0.5. This observation is directly related to the inability to accurately predict the detachment of the wall jet (boundary layer separation) (see Figs. 5 and 6). This discrepancy has been addressed by several other researchers in the past and also in Section 1 of this paper. Furthermore, the high levels of turbulent kinetic energy at x/L = 0.2 below y/L = 0.97 are the reason for the inability of the RNG k-ε model to predict a top-hat velocity profile. The high values of k smooth out the velocity profile in the outer region of the wall jet (y/L < 0.97), as can be seen in Figure 5d. The results of the LR k-ε, SST k-ω and the RSM model in general show a much better agreement with the turbulent kinetic energy profiles based on the measurements, although these models underpredict the value of k in the inner region of the wall jet at x/L = 0.2 (y/L ≈ 0.99) and at x/L = 0.5 (y/L ≈ 0.94). The RSM model underpredicts the turbulent kinetic energy in the outer region at x/L = 0.5.

The profiles of turbulent kinetic energy for Re ≈ 2,500 are shown in Figure 9a (x/L = 0.2) and Figure 9b (x/L = 0.5). It is shown that the RNG k-ε model again strongly overpredicts the turbulent kinetic energy in the wall jet region, although the discrepancy is smaller than for Re ≈ 1,000. At x/L = 0.2, the other three turbulence models slightly overpredict the turbulent kinetic energy in the wall jet region, although the RSM model provides fairly accurate results for the outer region of the wall jet at this location. Below the wall jet, the RSM model shows the best agreement with the experimentally obtained turbulent kinetic energy; the other models overpredict the value of k. The numerical results at x/L = 0.5 obtained with the LR k-ε, SST k-ω and the RSM model show a fair to good agreement with the measurement results, although the turbulent kinetic energy below the wall jet is slightly overpredicted by all models.

5. Influence on air exchange efficiency prediction

The influence of the turbulence model on the calculation of the air exchange efficiency has been assessed for this particular case. The air exchange efficiency ε_a is defined as:

$$\varepsilon_a = \tau_n / 2\overline{\tau} \tag{3}$$

with τ_n the nominal time constant, which is the shortest possible time it takes to replace the air, and $\overline{\tau}$ the volume average age of air (Etheridge and Sandberg 1996). In the case of perfect mixing the air exchange efficiency would be equal to 0.5, since the average age of air in the room would in this case be equal to the age of air at the exhaust (= nominal time constant). By solving a transport equation for a passive scalar in CFD it is possible to numerically determine the age of air inside the enclosure, enabling the calculation of the air exchange efficiency using CFD (e.g. Chanteloup and Mirade 2009, Hang and Li 2011). The turbulent Schmidt number for these simulations was set to $Sc_t = 0.7$.

Figure 10 shows the distribution of the age-of-air in the vertical center plane (z/L = 0.5) for Re ≈ 1,000 as obtained with the CFD simulations with the four turbulence models. Due to the overprediction of the turbulent kinetic energy by the RNG k-ε model (Fig. 8), both in the wall jet region as in the remainder of the domain, the age-of-air contours for this model (Fig. 10a) differ considerably from those obtained with the other three models. Due to the unrealistic high levels of turbulent kinetic energy the turbulent diffusivity is much higher, which results in a lower age-of-air. Consequently, the air exchange efficiencies in the occupied zone below the wall jet (indicated with dashed rectangles in Fig. 10) differ significantly for the four turbulence models that were tested; the difference between the RNG k-ε model and the LR k-ε model is (0.36-0.29)/0.29 = 24%, and the difference between the RNG k-ε model and RSM model is even larger, 44%. The computed air exchange efficiencies for Re ≈ 2,500 are: RNG k-ε: 0.29; SST k-ω: 0.23; LR k-ε: 0.25; RSM: 0.22. The largest difference is again present between the RNG k-ε model and the RSM model, namely (0.29-0.22)/0.22 = 32%.

6. Discussion

This paper presents the results of a numerical study on isothermal forced mixing ventilation at two transitional slot Reynolds numbers (Re ≈ 1,000 and Re ≈ 2,500). There are two topics that are addressed in this discussion: (1) differences with earlier studies; (2) limitations of this study and future work.

As mentioned in the introduction, Davidson et al. (2000) performed CFD simulations of transitional room airflow and concluded that steady RANS was not capable of providing accurate predictions for these types of flows. It was stated that only LES could provide good results. These statements by Davidson et al. (2000) are not fully in line with the findings presented in the current paper. There are several possible explanations for this apparent discrepancy. The first and probably most important one is the grid size, which is essential for accurately predicting the near-wall flow and boundary layer separation. The finer the grid near the top wall, the more accurately the boundary layer can be resolved. As a result of the increase in computational power it was possible to perform simulations in the present study with y^* values well below 1, which are most probably smaller than those in the study by Davidson et al. (2000), who used 307,200 cells, with 10 cells over the inlet height, for their simulations. The total number of cells in the present study was over 3.4 million with 56 cells over the inlet height. Note that Davidson et al. (2000) only tested the modified k-ω model by Peng et al. (1997). Furthermore, the experimental setup was different, and also the value of Re (= 600) studied by Davidson et al. (2000) was not the same as in the current study.

The present study also has important limitations. The first one concerns the turbulence inlet conditions, which were chosen according to the best available information. Future measurements should include detailed measurements of turbulence properties at the inlet to increase the accuracy of this boundary condition. Second,

this study focused on a flow pattern in which three different challenges for room airflow prediction act in a combined way; (1) transitional flow; (2) turbulence anisotropy; (3) adverse pressure gradients. As a result of this combination, it was not possible to thoroughly analyze the capability of the studied turbulence models for each of the individual challenges. Future work could focus on decomposition of the flow pattern and on analysis of individual flow features and on each of the three challenges separately. Third, only four turbulence models were assessed. There are numerous other linear and non-linear two-equation models, second-order closure models, etc. Future work will include more RANS turbulence models, as well as LES. Furthermore, future work will include a more extensive validation of these numerical models for a larger range of Re-values and other inlet heights and inlet geometries. The influence of cell size and turbulence intensity on the flow pattern and the point of separation will be studied in more detail. Based on the extension of the work as described above, future publications will provide general guidelines on the use of steady RANS for the prediction of room airflow, both for transitional and turbulent airflow. Fourth, the experiments and CFD simulations presented in this paper were conducted for an isothermal situation. Although the focus was on the ability of steady RANS to predict transitional ventilation flow, future research will also focus on non-isothermal room airflow. The inclusion of thermal effects will make the flow problem even more complex, but also more realistic. As a result of the temperature differences the overall turbulence level in the enclosure might increase, which can be beneficial for the steady RANS turbulence models as studied in this paper.

Finally, full-scale measurements of transitional ventilation flow will be conducted using laser Doppler anemometry (LDA). In addition to velocities and turbulence levels, pollutant concentrations will be measured, which will enable the experimental determination of the air exchange efficiency.

7. Conclusions

This paper reports 3D steady RANS CFD simulations of isothermal forced mixing ventilation driven by a transitional wall jet for two slot Reynolds numbers (i.e. $Re \approx 1{,}000$ and $Re \approx 2{,}500$). Studies on transitional airflow in buildings are to the knowledge of the authors very scarce, and this paper aims on enhancing the knowledge of the numerical modeling of these types of flows. The flow pattern studied can be seen as challenging due to the presence of (1) transitional flow, (2) turbulence anisotropy (e.g. in the wall jet), (3) an adverse pressure gradient. The CFD simulations were validated using time-averaged PIV measurement results that were conducted in a reduced-scale water-filled experimental setup. Visualizations presented in a previous study (van Hooff et al. 2012a) have shown that the flow is transitional for the combination of a slot height $h/L = 0.1$ and for these Re-values. The CFD simulations were conducted with four different turbulence models (RNG k-ε, SST k-ω, LR k-ε and a RSM model). The following conclusions can be made:

- Although most turbulence models are developed for fully developed turbulent flow, the results obtained with the LR k-ε and SST k-ω models show a fair to good agreement with the measurement results. In general, the results obtained with the LR k-ε model show the best agreement for this specific case.
- The flow pattern obtained with the RNG k-ε turbulence model shows large deviations with the measured flow pattern due to the inability of this model to predict the flow separation due to the adverse pressure gradient. The reason for this inability is the unrealistically high level of turbulent kinetic energy in the wall jet region.
- Although the velocity profiles obtained with the RSM model show a fair to good agreement, the prediction of the large recirculation zone in the cube deviates quite a lot from the measurements.
- The prediction of the turbulent kinetic energy shows a fair to good agreement for the SST k-ω, LR k-ε and RSM model. The RNG k-ε model largely overpredicts the turbulent kinetic energy in the wall jet region. This overprediction results in a delayed separation of the wall jet due to the adverse pressure gradient.
- Although the studied configuration is highly complex due to the presence of transitional flow, an adverse pressure gradient, and a wall jet which is intrinsically anisotropic, two out of four turbulence models provide quite accurate results.
- As a result of the differences in predicted flow pattern and turbulent kinetic energy levels the calculated air exchange efficiencies in the occupied zone show relatively large differences between the RNG k-ε model on the one hand, and the SST k-ω, Low-Re k-ε and RSM models on the other hand. The differences between the predictions obtained with the different models can be as large as 44%.

The last conclusion illustrates that large differences can be present when performing the same study with different turbulence models. Caution should be taken in the process of choosing the computational methods and

models to avoid erroneous ventilation predictions. Additional comparative studies are needed to evaluate the validity of the present findings beyond the slot height (h/L = 0.1), Re-values and slot geometry investigated here, and to test other computational parameters that might influence the predicted flow pattern, e.g. grid size/distribution, boundary conditions, turbulence models.

8. Acknowledgements

Twan van Hooff is currently a PhD student funded by both Eindhoven University of Technology in the Netherlands and Fonds Wetenschappelijk Onderzoek (FWO) - Flanders, Belgium (FWO project number: G.0435.08). The FWO Flanders supports and stimulates fundamental research in Flanders. Its contribution is gratefully acknowledged. The authors are grateful for the valuable comments and discussions with Shijie Cao and Prof. Johan Meyers (KU Leuven), partners in the FWO project.

The measurements reported in this paper were supported by the Laboratory of the Unit Building Physics and Services (BPS) at Eindhoven University of Technology and the Laboratory of Building Physics at the KU Leuven.

9. References

Awbi, H.B., (1989) Application of computational fluid dynamics in room ventilation, *Building and Environment*, (24)1, 73-84.

Awbi, H.B., (2007) *Ventilation Systems - Design and performance*. Taylor & Francis, New York.

Baker, A.J., Williams, P.E., Kelso, P.E., (1994) Numerical calculation of room air motion – part 1: math, physics and CFD modelling, *AHSRAE Transactions*, 100(1), 515-530.

Cao, S.-J., Meyers, J., (2012) On the construction and use of linear low-dimensional ventilation models, *Indoor Air, 22, 427-441*..

Casey, M., Wintergerste, T. (Eds). Best Practice Guidelines, ERCOFTAC Special Interest Group on Quality and Trust in Industrial CFD, ERCOFTAC, Triomflaan 43, B-1160, Brussels; 2000.

Chang, K.C., Hsieh, W.D., Chen, C.S., (1995) A modified low-Reynolds-number turbulence model applicable to recirculating flow in pipe expansion, *Journal of Fluids Engineering*, 117, 417–423.

Chanteloup, V., Mirade, P.S,. (2009) Computation fluid dynamics (CFD) modeling of local mean age distribution in forced food plants, *Journal of Food Engineering*, 90, 90–103.

Chen, Q., Jiang, Z., (1992) Significant questions in predicting room air motion, *AHSRAE Transactions*, 98 (Pt. 1), 929–939.

Chen, Q., (1995) Comparison of different k-ε models for indoor air-flow computations, *Numerical Heat Transfer Part B: Fundamentals*, 28, 353-369.

Chen, Q., (1996) Prediction of room air motion by Reynolds-stress models, *Building and Environment*, 31, 233-244.

Chen, Q., (2009) Ventilation performance prediction for buildings: A method overview and recent applications, *Building and Environment*, 44, 848-858.

Chen, Q., Srebric, J., (2002) A procedure for verification, validation, and reporting of indoor environment CFD analyses, *HVAC&R Research*, 8(2), 201-16.

Davidson, L., Nielsen, P.V., Topp, C., (2000) Low Reynolds number effects in ventilated rooms: a numerical study, *Proc. of Roomvent 2000*, Oxford, 307-312.

Etheridge, D.W., Sandberg, M., (1996) *Building Ventilation: Theory and Measurement*. London: Wiley.

Fluent Inc. (2006) *Fluent 6.3 user's guide*, Lebanon.

Gan, G., Awbi, H.B., (1994) Numerical simulation of the indoor environment, *Building and Environment*, 29(4), 449-459.

Hanjalić, K., (1994) Advanced turbulence closure models: a view of current status and future prospects, *International Journal of Heat and Fluid Flow*, 15(3), 178–203.

Hang, J., Li, Y., (2011) Age of air and air exchange efficiency in high-rise urban areas and its link to pollutant dilution, *Atmospheric Environment*, 45, 5572-5585.

Jones, P.J., Whittle, G.E., (1992) Computational fluid dynamics for building air flow prediction. Current status and capabilities, *Building and Environment*, 27(3), 321-338.

Kato, S., Murakami, S., Mochida, A., Akabayashi, S., Tominaga, Y., (1992) Velocity–pressure field of cross ventilation with open windows analyzed by wind tunnel and numerical simulation, *Journal of Wind Engineering and Industrial Aerodynamics*, 44, 2575–2586.

Launder, B.E., Spalding, D.B., (1974) The Numerical Computation of Turbulent Flows, *Computer Methods in Applied Mechanics and Engineering*, 3, 269-289.

Li, Y., Nielsen, P.V., (2011) CFD and ventilation research, *Indoor Air*, 21, 442-453.
Menter, F.R., (1993) Zonal two equation k-ω turbulence models for aerodynamic flows, *AIAA Paper,* 93-2906.
Menter, F.R., (1994) Two-equation eddy-viscosity turbulence models for engineering applications. *AIAA Journal*, 32, 1598–1605.
Menter, F.R. (1996) A comparison of some recent eddy-viscosity turbulence models, *Journal of Fluids Engineering*, 118, 514–519.
Moureh, J., Flick, D., (2003) Wall air-jet characteristics and airflow patterns within a slot ventilated enclosure, *International Journal of Thermal Sciences*, 42, 703-711.
Moureh, J., Flick, D., (2005) Airflow characteristics within a slot-ventilated enclosure, *International Journal of Heat and Fluid Flow*, 26, 12-24.
Murakami, S., Kato, S., Ooka, R., (1994) Comparison of numerical predictions of horizontal non-isothermal jet in a room with three turbulence models – k-ε EVM, ASM, and DSM, *ASHRAE Transactions*, 100(2), 697–706.
Nielsen, P.V., (1973) Berechnung der Luftbewegung in einem zwangsbelüfteten Raum, *Gesundheits-Ingenieur*, 94, 299-302.
Nielsen, P.V., (1990) Specification of a two-dimensional test case, Aalborg University, *IEA Annex 20: Air Flow Patterns within Buildings*.
Nielsen, P.V., (1998) The selection of turbulence models for prediction of room airflow, *ASHRAE Transactions*, 104(1B), 1119-1127.
Nielsen, P.V., (2004) Computational fluid dynamics and room air movement. *Indoor Air*, 14, 134-143.
Nielsen, P.V., Filholm, C., Topp, C., Davidson, L., (2000) Model experiments with low Reynolds number effects in a ventilated room, *Proc. of Roomvent 2000*, Oxford, 185-190.
Norton, T., Sun, D.-W., Grant, J., Fallon, R., Dodd, V., (2007), Applications of computational fluid dynamics (CFD) in the modelling and design of ventilation systems in the agricultural industry: A review, *Bioresource Technology*, 98, 2386–2414.
Patel, V.C., Rodi, W., Scheuerer, G., (1985) Turbulence models for near-wall and low Reynolds number flows: a review, *AIAA Journal*, 23, 1308–1319.
Peng, S.-H., Davidson, L., Holmberg, S., (1997) A modified low-Reynolds-number k-ω model for recirculating flows, *Journal of Fluids Engineering*, 119, 867-875.
Ramponi, R., Blocken, B., (2012) CFD simulation of cross-ventilation for a generic isolated building: impact of computational parameters, *Building and Environment*, 53, 34-48.
Rodi, W., Scheuerer, G., (1986), Scrutinizing the k-ε turbulence model under adverse pressure gradient conditions, *Journal of Fluids Engineering*, 108, 174-179.
Schälin, A., Nielsen, P.V., (2004) Impact of turbulence anisotropy near walls in room airflow, *Indoor Air*, 14, 159–168.
Sørensen, D.N., Nielsen, P.V., (2003) Quality control of computational fluid dynamics in indoor environments, *Indoor Air*, 13(1), 2-17.
van Hooff, T., Blocken, B., (2010) Coupled urban wind flow and indoor natural ventilation modelling on a high-resolution grid: A case study for the Amsterdam ArenA stadium, *Environmental Modelling & Software*, 25(1), 51-65.
van Hooff, T., Blocken, B., Defraeye, T., Carmeliet, J., van Heijst, G.J.F., (2012a) PIV measurements of a plane wall jet in a confined space at transitional slot Reynolds numbers, *Experiments in Fluids*, 53(2), 499-517.
van Hooff, T., Blocken, B., Defraeye, T., Carmeliet, J., van Heijst, G.J.F., (2012b) PIV measurements and analysis of transitional flow in a reduced-scale model: ventilation by a free plane jet with Coanda effect, *Building and Environment*, 56, 301-313.
van Hooff, T., Blocken, B., Aanen, L., Bronsema, B., (2012c) Numerical analysis of the performance of a venturi-shaped roof for natural ventilation: influence of building width, *Journal of Wind Engineering and Industrial Aerodynamics*, 104-106, 419-427.
Wang, M., Chen, Q., (2009) Assessment of various turbulence models for transitional flows in enclosed environment, *HVAC&R Research*, 15(6), 1099-1119.
Wang, M., Chen, Q., (2010) On a hybrid RANS/LES approach for indoor airflow modeling, *HVAC&R Research*, 16(6), 731-747.
Wilcox, D.C., (1993) Comparison of two-equation turbulence models for boundary layers with pressure gradient, *AIAA Journal*, 31(8), 1414-1421.
Wilcox, D.C., (1998) *Turbulence Modeling for CFD*. DCW Industries, Inc., La Canada, California.
Yakhot, V., Orszag, S.A., Thangam, S., Gatski, T.B., Speziale, C.G., (1992) Development of turbulence models for shear flows by a double expansion technique, *Physics of Fluids A*, 4, 1510-1520.
Zhai, Z., Zhang, Z., Zhang, W., Chen, Q., (2007) Evaluation of various turbulence models in predicting airflow and turbulence in enclosed environments by CFD: part 1 –summary of prevalent turbulence models, *HVAC&R Research*, 13(6), 853–870.

Zhang, Z., Zhang, W., Zhai, Z., Chen, Q., (2007) Evaluation of various turbulence models in predicting airflow and turbulence in enclosed environments by CFD: part 2 – comparison with experimental data from literature, *HVAC&R Research*, 13(6), 871–886.

TABLE

Table 1: Grids used for the grid-sensitivity analysis.

Grid	Number of cells [-]	y^* (top surface; min) [-]	y^* (top surface; max) [-]
Coarse	1,254,400	0.045	0.45
Middle	3,437,056	0.026	0.40
Fine	10,022,400	0.007	0.28

FIGURE CAPTIONS

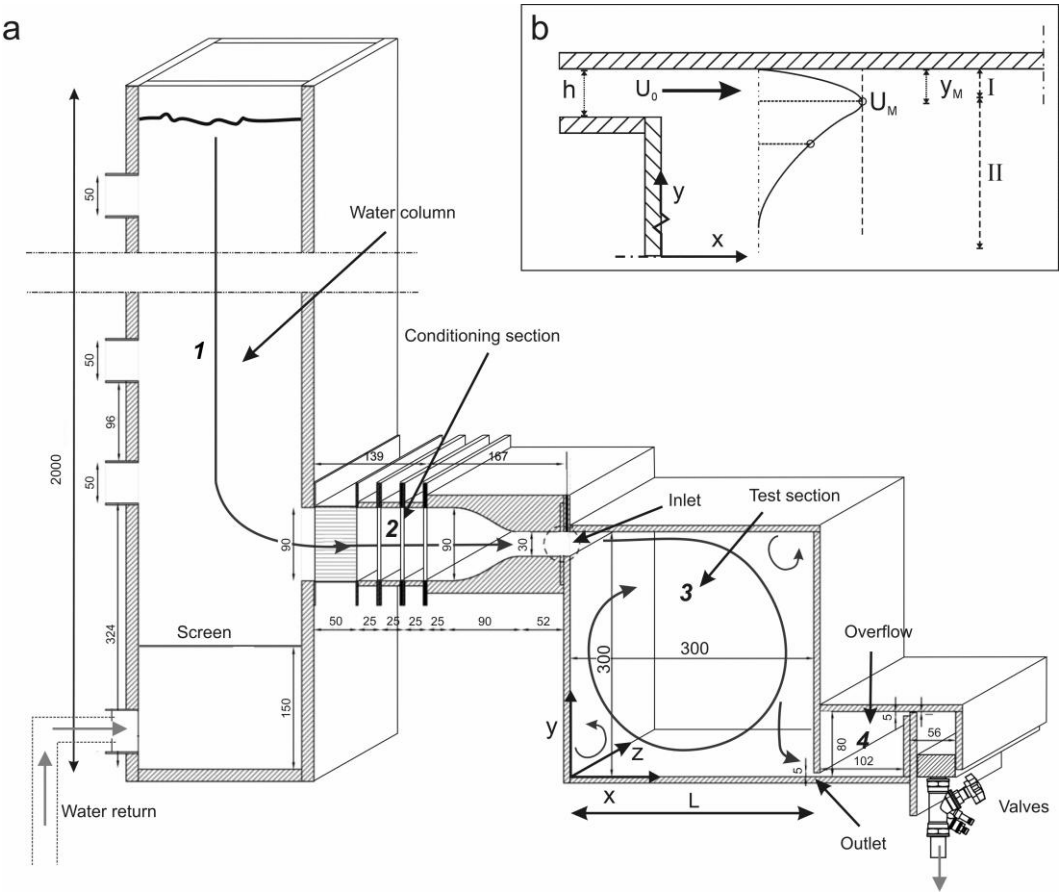

Fig. 1: (a) Reduced-scale setup used for the flow visualizations and PIV measurements (1) water column; (2) flow conditioning section in front of the inlet, (3) test section, (4) overflow, and the valves that are placed in a block after the overflow. Dimensions in mm. (b) 2D schematic representation of the plane wall jet with I the inner region, II the outer region, U_M the maximum velocity, y_M the distance from the top wall to the location of U_M.

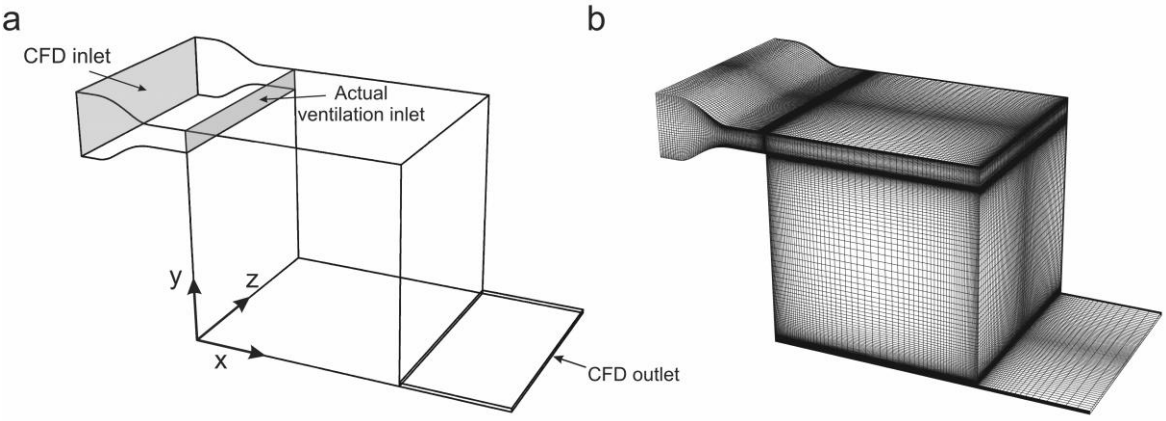

Fig. 2: (a) Computational model of the water cube. (b) Computational grid (coarse grid: 1.25 million cells).

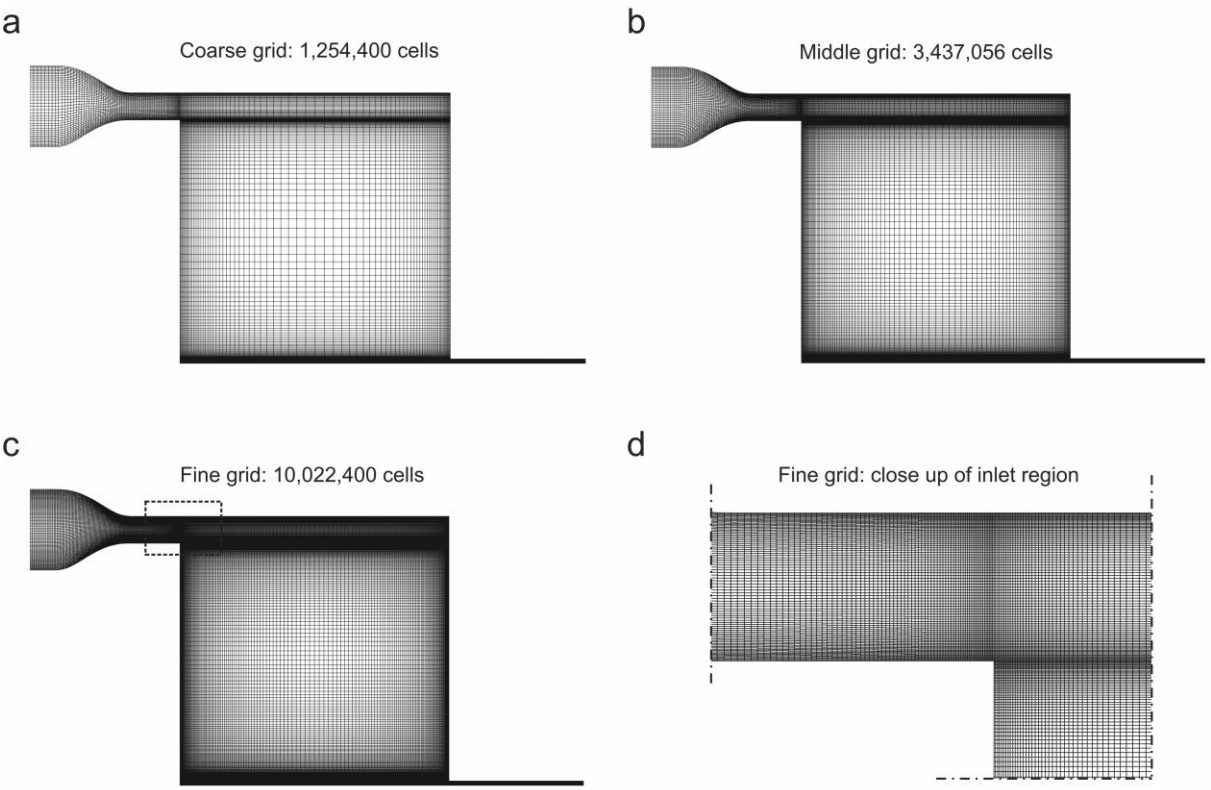

Fig. 3: Computational grids used for the grid-sensitivity analysis: (a) coarse grid (1,254,400 cells); (b) middle grid (3,437,056 cells); (c) fine grid (10,022,400 cells). (d) Enlarged figure of the mesh in the inlet region (fine grid).

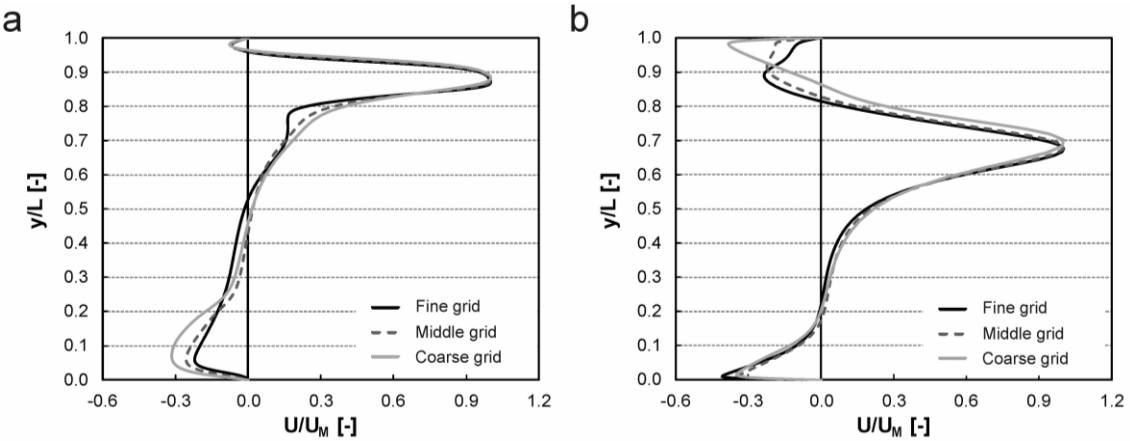

Fig. 4: Results of the grid-sensitivity analysis: (a) U/U_M at x/L = 0.5; (b) U/U_M at x/L = 0.8.

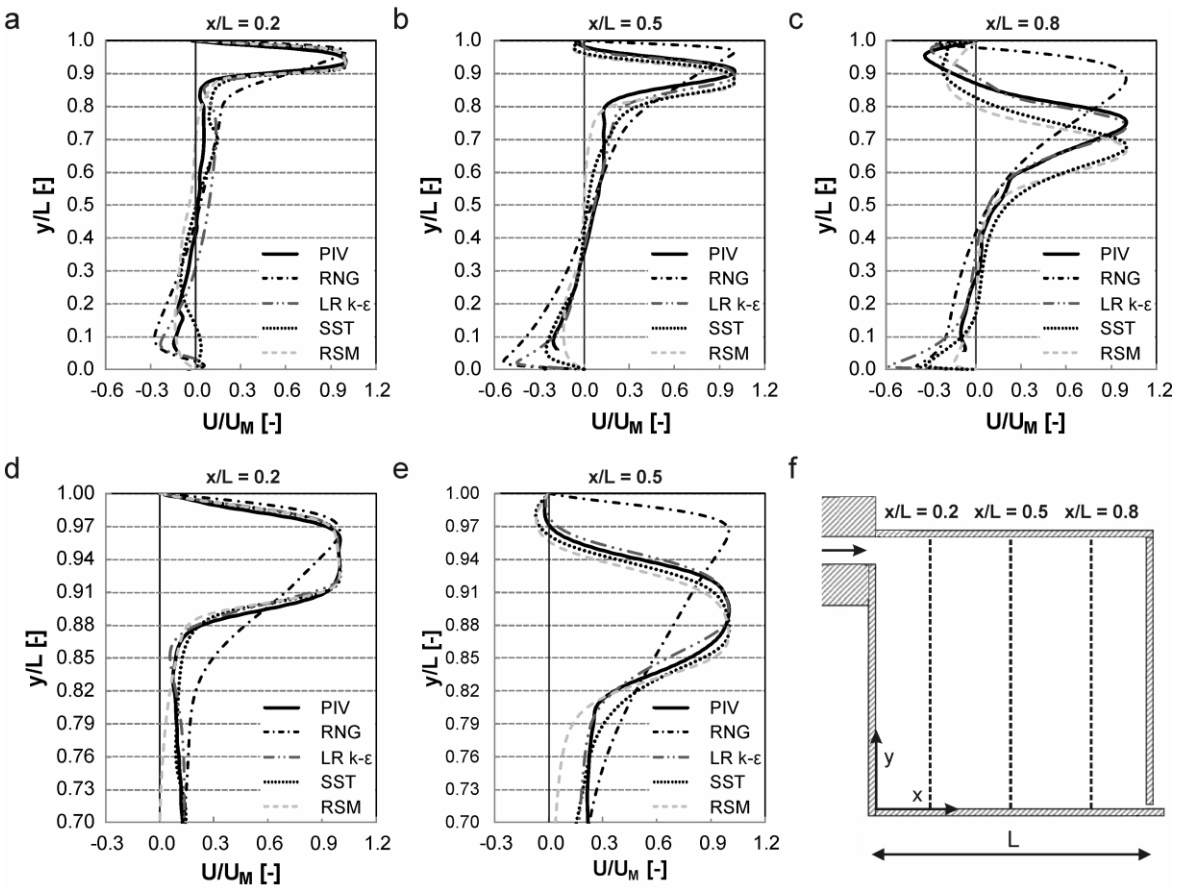

Fig. 5: (a-c) Comparison of PIV results in ROI1 with CFD simulation results for Re ≈ 1,000: (a) U/U_M at x/L = 0.2; (b) U/U_M at x/L = 0.5; (c) U/U_M at x/L = 0.8. Comparison PIV results in ROI2 with CFD simulation results: (d) U/U_M at x/L = 0.2; (e) U/U_M at x/L = 0.5. (f) Locations of x/L = 0.2, 0.5 and 0.8.

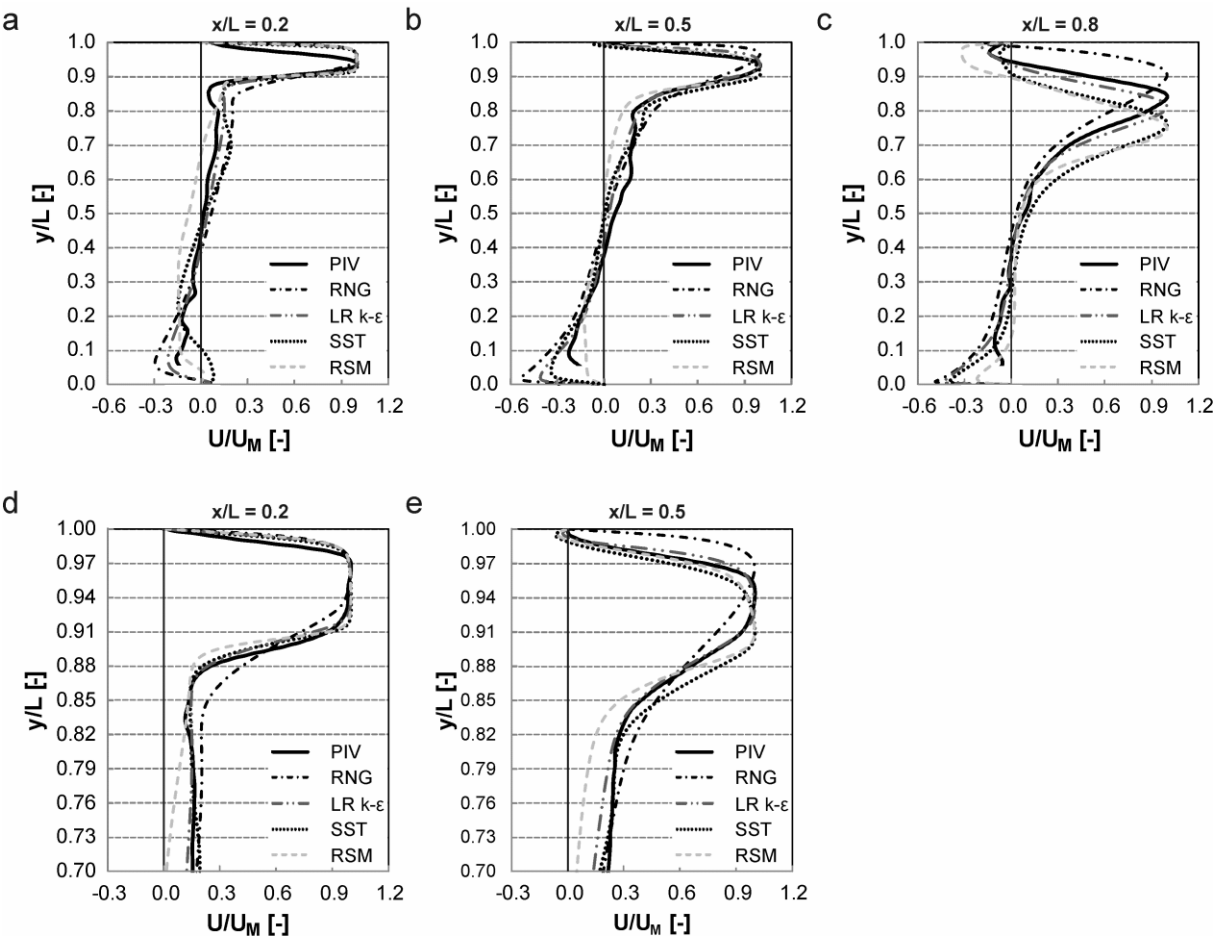

Fig. 6: (a-c) Comparison of PIV results in ROI1 with CFD simulation results for Re ≈ 2,500: (a) U/U_M at x/L = 0.2; (b) U/U_M at x/L = 0.5; (c) U/U_M at x/L = 0.8. Comparison PIV results in ROI2 with CFD simulation results: (d) U/U_M at x/L = 0.2; (e) U/U_M at x/L = 0.5.

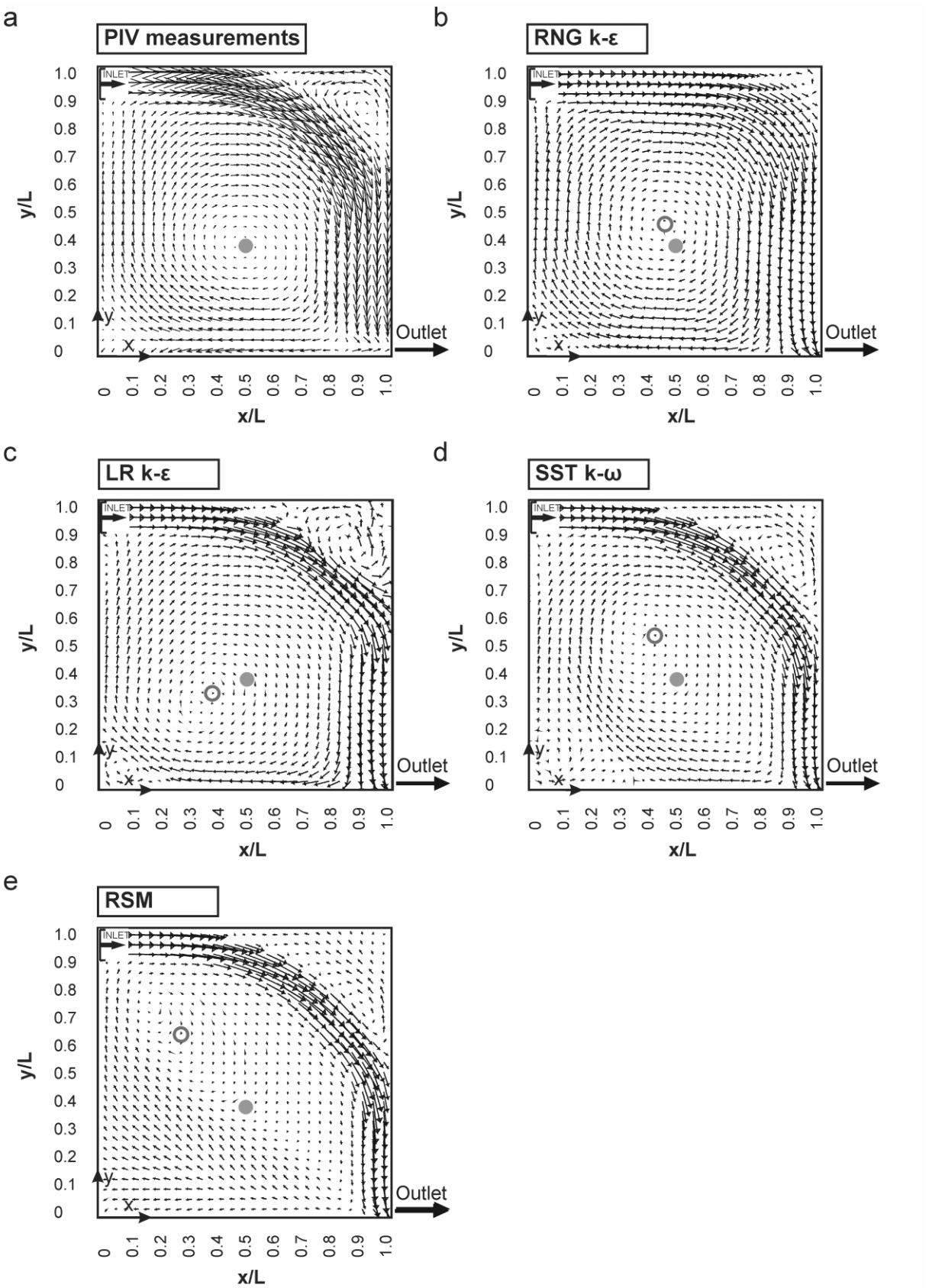

Fig. 7: Time-averaged velocity vector fields in the vertical center plane for Re ≈ 1,000. (a) PIV measurements; (b) RNG k-ε; (c) LR k-ε; (d) SST k-ω; (e) RSM. ● = measured center of the large recirculation zone, ○ = computed center of large recirculation zone.

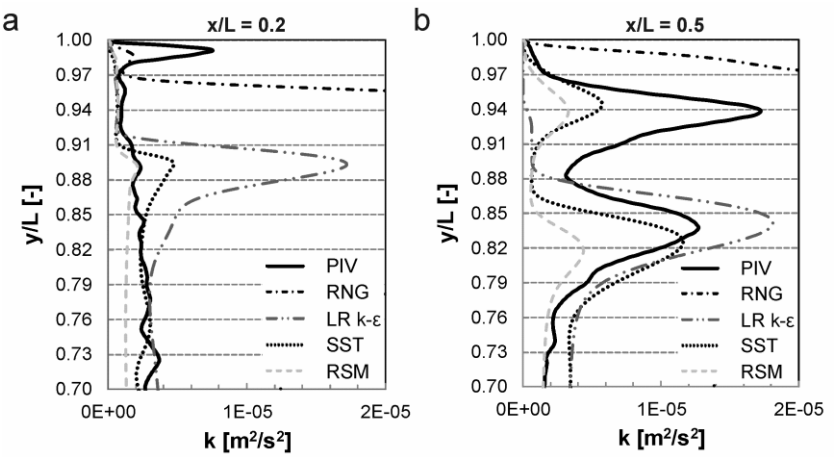

Fig. 8: Comparison of measured turbulent kinetic energy k and values obtained from CFD simulations for Re ≈ 1,000: (a) k at x/L = 0.2; (b) k at x/L = 0.5. The values of k for the RNG model do not entirely fall in the range of the graphs ($k_{max} = 10^{-4}$ m^2/s^2 at x/L = 0.2; $k_{max} = 7 \times 10^{-5}$ m^2/s^2 at x/L = 0.5).

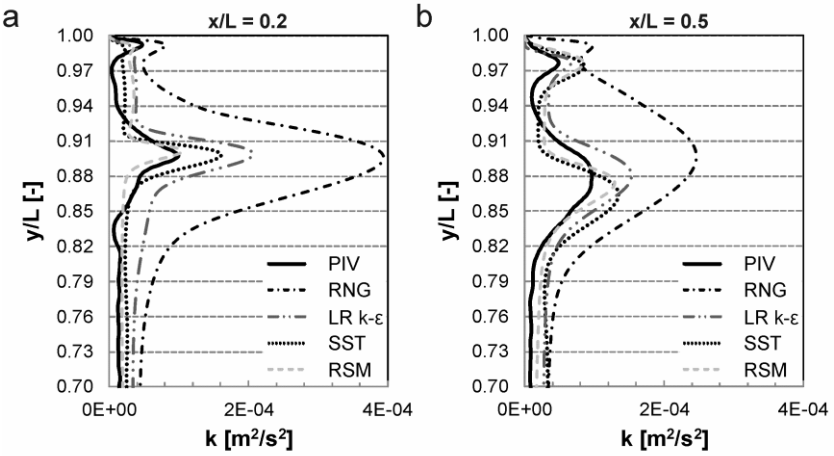

Fig. 9: Comparison of measured turbulent kinetic energy k and values obtained from CFD simulations for Re ≈ 2,500: (a) k at x/L = 0.2; (b) k at x/L = 0.5.

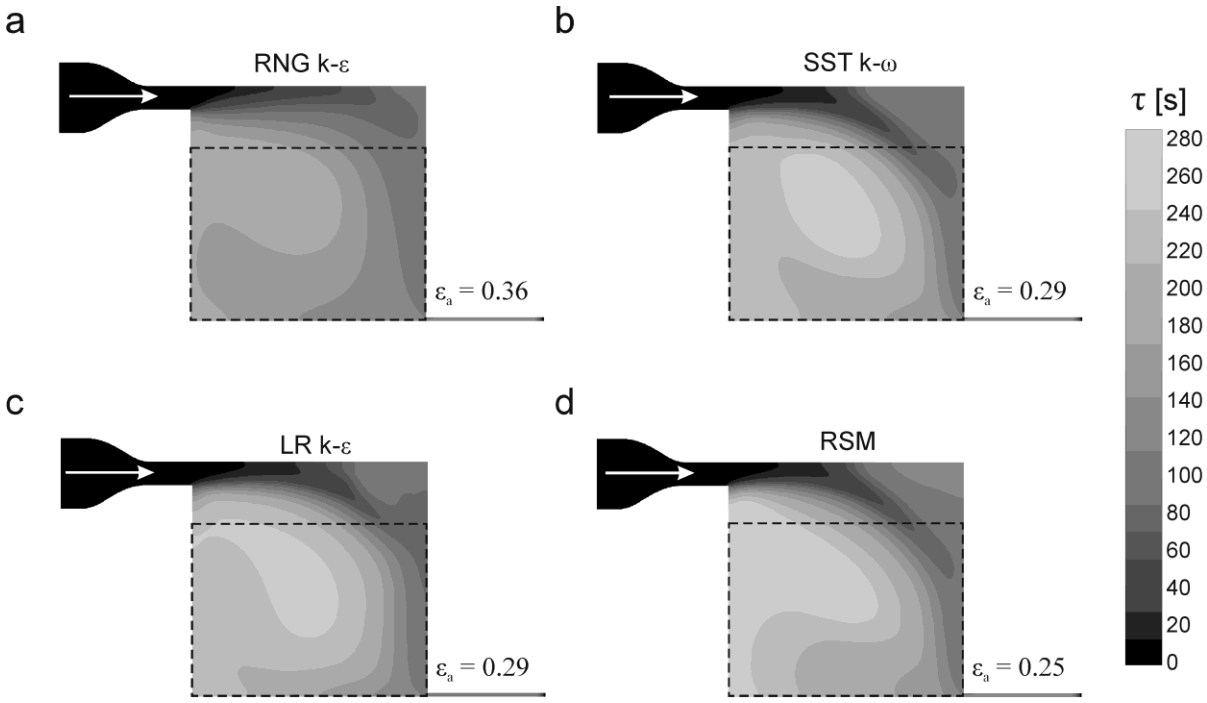

Fig. 10: Contours of computed age of air in the occupied zone (indicated with the dashed rectangle) and value of the air exchange efficiency for Re ≈ 1,000. (a) RNG k-ε model; (b) SST k-ω model; (c) LR k-ε model; (d) RSM model.